2×2-slot Element for 60GHz Planar Array Antenna Realized on Two Doubled-sided PCBs Using SIW Cavity and EBG-type Soft Surface fed by Microstrip-Ridge Gap Waveguide

2×2-slot Element for 60GHz Planar Array Antenna Realized on Two Doubled-sided PCBs Using SIW Cavity and EBG-type Soft Surface fed by Microstrip-Ridge Gap Waveguide

Seyed Ali Razavi, Per-Simon Kildal, *Fellow, IEEE*, Liangliang Xiang, Esperanza Alfonso, Haiguang Chen

***Abstract*—A wideband 2×2-slot element for a 60 GHz antenna array is designed by making use of two double-sided printed circuit boards (PCBs). The upper PCB contains the four radiating cavity-backed slots, where the cavity is formed in substrate-integrated waveguide (SIW) using metalized via holes. The SIW cavity is excited by a coupling slot. The excitation slot is fed by a microstrip-ridge gap waveguide formed in the air gap between the upper and lower PCBs. The lower PCB contains the microstrip line, being short-circuited to the ground plane of the lower PCB with via holes, and with additional metalized via holes alongside the microstrip line to form a stopband for parallel-plate modes in the air gap. The designed element can be used in large arrays with distribution networks realized in such microstrip-ridge gap waveguide technology. Therefore, the present paper describes a generic study in an infinite array environment, and performance is measured in terms of the active reflection coefficient S11 and the power lost in grating lobes.**

The study shows that the radiation characteristics of the array antenna is considerably improved by using a soft surface EBG-type SIW corrugation between each 2×2-slot element in E-plane to reduce the mutual coupling.

The study is verified by measurements on a 4×4 element array surrounded by dummy elements and including a transition to rectangular waveguide WR15.

***Index Terms*— gap waveguide, slot antenna array, soft and hard surfaces, EBG surface, substrate integrated waveguide (SIW).**

I. Introduction

SLOT ARRAY antennas are an interesting type of antennas that has been widely used in radar and communication applications at which high gain and narrow radiation patterns are required. When hollow waveguide corporate distribution network feeds the slots, high radiation efficiency can be achieved since the transmission loss is very low. In [1-5] slot array antennas with different hollow waveguide corporate distribution networks have been described for millimeter waves. The present paper deals with realizing antennas of similar performance using PCB technology at 60 GHz (Fig. 1).

In [1] an aperture efficiency of 51% is achieved over a 9.5% (40~43.8GHz) bandwidth for a 24×24 slot array, but the proposed rectangular waveguide distribution network has a complicated structure that is expensive to manufacture. In order to improve this, an alternative single layer distribution network was proposed in [2]. As a result the aperture efficiency became larger (65%), but over a much narrower bandwidth due to long line effects (i.e. different time-delays). By modifying the proposed distribution network in [2], even wider impedance bandwidth was achieved, but the efficiency reduced to 46% [3].

The corporate distribution networks in [2-3] are single layer rectangular waveguide structures. By a multi layer distribution network it is possible to provide a wider bandwidth, but cost and complexity increase. In [4] a slot array antenna with a double-layer distribution network is proposed, providing a bandwidth of 15.4% (11~12.7GHz) and efficiency of 85%. This slot array is composed of several 2×2-slot cavity-backed subarrays, and each cavity is excited by the waveguide at the lower layer through a coupling slot. In [5] the array is a modified form of that presented in [4], composed of several 2×2-slot cavity-backed subarrays. In addition, the spacing between the slots is constant and smaller than a free-space wavelength, so there are no grating lobes if the slots are correctly excited. In [5] an excellent performance is reported with bandwidth of 12% (58.2~65.2GHz), aperture efficiency of 93.7% and total efficiency of 83.3%.

The present paper aims at realizing a similar 2×2-slot element as in [5] for operation between 57 and 66 GHz, by using two double-sided PCBs. The backed cavity of the 2×2-slot element is implemented in the upper PCB using substrate integrated waveguide (SIW) technology, and the distribution network is implemented in the airgap between the upper and lower PCBs using gap waveguide technology with the lower PCB constituting the textured surface, see Fig. 2.

Ali.Razavi is visting PhD student at Chalmers University of Technology, He is now with graduate university of advanced technology, Kerman, Iran.

P.-S. Kildal is with Chalmers University of Technology, Gothenburg, Sweden. Liangliang Xiang is with Huawei, Shanghai, China. Haiguang Chen is with Huawei Sweden AB. Gothenburg, Sweden. Esperanza Alfonso is with Gapwaves AB, Gothenburg, Sweden.

The work has been supported in part by Huwei Technologies Sweden AB via a project to Gapwaves AB, Gothenburg, Sweden, and makes use of basic gap waveguide technology developed mainly on a project supported by Swedish Research Council VR.

In all the structures presented in [1-5], the distribution network is a hollow rectangular waveguide structure. The major advantage of hollow waveguides compared to microstrip lines is the lower transmission loss since the waveguides do not suffer from dielectric loss and radiation loss present when using microstrip lines. This advantage becomes bigger in larger arrays and at higher frequencies, but then it becomes more difficult to meet the required higher precision of the manufacturing process. In particular, it becomes difficult to achieve good conductive contact between the metal parts used to realize the hollow waveguide structures themselves. The antenna in the present paper makes use of two parallel PCBs to realize the topology of the same distribution network with no requirement of conductive contact between the two PCBs that are separated by a small air gap. This is possible by using PCB-based ridge gap waveguide and SIW technologies.

The gap waveguide technology was introduced in 2009 as an alternative to hollow waveguides and microstrip lines at high frequencies with performance close to rectangular waveguides if the dimensions are properly chosen [6-7]. The gap waveguides are realized between two parallel flat metal surfaces, one of them with a texture, and there is no need for electrical contact between them. This represents a manufacturing advantage in particular for millimeter waves. The transmission line is realized in the narrow gap between the two surfaces by means of the texture. The wave propagation appears along smooth guiding parts like metal grooves, ridges or strips in the textured surface, and it is stopped in other directions by quasi-periodic texture-parts that provide a cut-off for other parallel-plate modes within a stopband. Based on this principle three different versions of gap waveguides called ridge, groove and microstrip gap waveguides were presented in [8] and verified experimentally in [9], [10] and [11-12], respectively. The last two papers verify two different microstrip gap waveguide types, referred to as a) *inverted* or *suspended* microstrip gap waveguide [11] and b) *microstrip-ridge* gap waveguide [12]. The present paper makes use of the latter microstrip-ridge gap waveguide to feed the 2×2-slot array element, see Fig. 2.

This quasi-periodic texture of a gap waveguide works in principle like a high impedance surface (ideally a perfect magnetic conductor). It is preferable realized by metal pins, but microstrip patches with via holes can also be used [13]. The present paper makes use of metallized via holes with small circular patches on the top acting almost like pins (or mushroom surfaces).

Within the stopband of the parallel-plate waveguide created by the periodic structure, the wave propagation in groove gap waveguide is similar to that of rectangular waveguide, and in ridge and microstrip versions it resembles that of inverted (also called suspended) microstrip lines [14].

The gap waveguides originate from artificially soft and hard surfaces. This concept was defined in 1988, and updated and related to electromagnetic bandgap (EBG) surfaces and modern metamaterials in [15]. We will here also investigate the use of the soft surface in the form of a single SIW-corrugation to reduce the mutual coupling between each 2×2-slot subarray, similar to how this was used in [16]. This could also have been done with a planar double-periodic EBG surface [17], but the bandwidth is normally larger with soft surfaces.

The present work is part of a larger project to realize a 60 GHz high-gain antenna using PCB technology. The size we aim at, is an array with 32×32 slot elements, i.e. 16×16 array of 2×2-slot elements and a fully branched or corporate distribution network in microstrip-ridge gap waveguide technology. The distribution network and manufacturing issues will be discussed in a future paper. In order to verify the 2×2-slot element we chose to manufacture a 4×4 slot array, i.e. a 2×2 array of our 2×2-slot cavity-backed subarrays. We have presently included some measurements of this antenna, but without any description of the distribution network that will be included in the future paper.

We should also here mention two other papers about directive gap waveguide antennas. One is a 4×4 horn array ($2\lambda \times 2\lambda$ horn size) with corporate distribution network in inverted microstrip gap waveguide (without via holes) backed by a uniform grid of metal pins [18]. The other is an all-metal ridge gap waveguide slot array [19].

II. Antenna Configuration And Design

Figs. 1 and 2 show drawings of the studied antenna consisting of two double-sided PCBs with an air gap between them. The upper metal layer of the upper PCB has an array of radiating slots, in the example shown as 8×8 slots. These form 4×4 equal subarrays, each consisting of 2×2 slots, referred to as a 2×2-slot subarray. The 2×2-slot subarray is shown in distributed 3-D view in Fig. 2, which clearly illustrates the two double-sided PCBs. The subarrays are in E-plane (yz-plane) separated by long slots extending from one edge of the antenna to the opposite. They work as corrugations, to be explained below. The distribution network is formed by the microstrip-ridge gap waveguide between the upper and lower PCBs, and there is a coupling slot in the lower ground plane of the upper PCB that provides the coupling between the feed

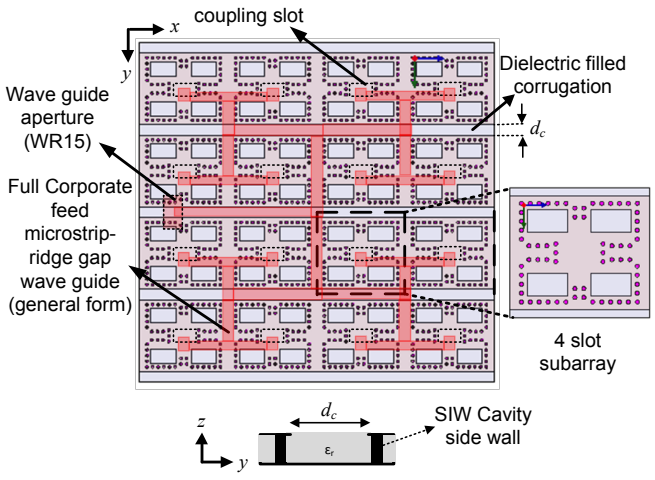

Fig. 1. Example of a PCB-based array antenna consisting of 8×8 radiating slots. It consists of 4×4 subarrays, and each subarray consists of 2×2 slots. The 2×2-slot subarray is shown separately.

network and the 2×2-slot subarray. The radiating slots are uniformly spaced in both *x* and *y* directions with distances smaller than, but close to, one wavelength, in order to minimize the grating lobe level at the same time as the aperture is kept as large as possible to get the highest gain possible.

A. The 2×2-slot subarray and numerical approach

The cavity below the four radiating slots of each subarray is realized by via holes, i.e. SIW technology. The cavity configuration is similar to that in [5], but in our case it is

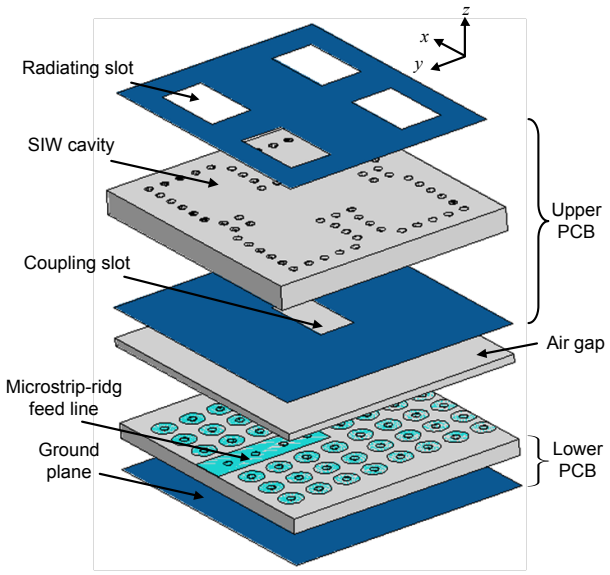

Fig. 2. Distributed 3-D view of 2×2-slot subarray of the antenna in Fig. 1. It consists of 2 PCBs separated by an air gap. The upper PCB has two ground planes with slots, and the lower PCB has one ground plane and an upper textured surface with strips and circular patches

dielectric-filled and realized by SIW in the same way as for the crossed-slot case in [20]. In the present paper the focus is on the design of the 2×2-slot subarray, taking mutual coupling between subarrays into consideration. This is done by assuming an infinite two-dimensional array and modeling this by applying periodic walls around the 2×2-slot subarray. The periodic boundary model in HFSS is standard corresponding for our case to perfect electric conducting walls in E-plane and perfect magnetic conducting walls in H-plane, and we apply them only to the upper PCB. The aim is to design the subarrays in such a way that the aperture efficiency of the 32×32 slot array is high and the input reflection coefficient S_{11} low over as wide bandwidth as possible. We used the commercial Ansoft HFSS high frequency solver in the design process. First, we assumed that the cavity had solid metal walls, defined by the dimensions shown in Fig. 3(a), and thereafter we replaced them by via holes. In the SIW cavity the spacing between via holes is smaller than $\lambda_c/10$, where λ_c is wavelength in the substrate, so that the leakage through the cavity sidewalls becomes negligible [21-23]. At the same time, the spacing between via holes should be chosen so that the minimum number of vias is used in order to simplify the construction process. In this work we also tried to minimize the number of via holes in the SIW cavity to make the manufacturing cost as low as possible. The thickness of the PCB with the SIW cavity should be small enough to ensure a single-mode in the cavity. As illustrated in Fig. 3(a), the feed line is extended to the center of the coupling slot.

B. The microstrip-ridge gap waveguide

The distribution network is implemented in the air-filled gap between the upper and lower PCBs. Initially we wanted to use a suspended microstrip gap waveguide, i.e. a suspended microstrip network, in which the microstrip line is supported by a substrate, with a regular grid of metal pins below the substrate, like in the antenna in [18]. However, in our application, the final antenna needs a WR15 rectangular waveguide port connected to the back plane of the lower PCB. And, we found it impossible to design a wideband transition from a vertical WR15 waveguide to the suspended microstrip gap waveguide, whereas it could be done using microstrip-ridge gap waveguide. The inverted microstrip line of the microstrip-ridge gap waveguide is provided with via holes to the ground plane of the lower PCB, and these have spacing closer than half wavelength in the substrate, in order to prevent the excitation of fields in the substrate below the

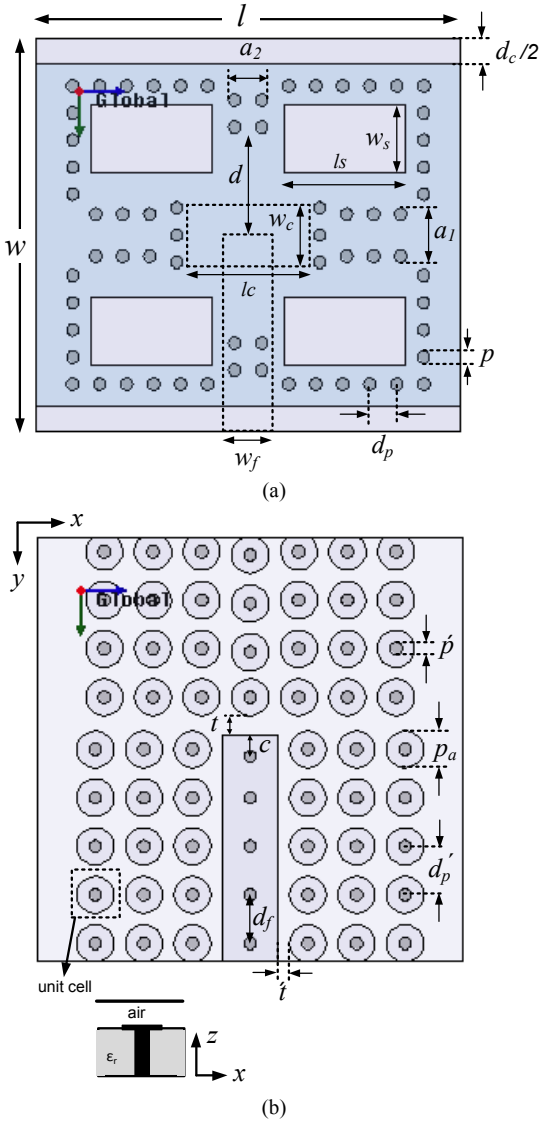

Fig. 3. Geometrical parameters of a 2×2-slot subarray. (a). Upper PCB including the coupling slot. The position of feed line relative to the coupling slot is also indicated. (b). Lower PCB including high impedance surface with a microstrip-ridge line ending in the middle of the coupling slot.

inverted microstrip line.

The microstrip-ridge gap waveguide in [13] makes use of so-called mushrooms (metal patches with metalized via holes connecting them to the ground plane) in the PCB to obtain the stopband for parallel-plate modes. In the present 60 GHz application we are able to realize a stopband with metalized via-holes without the patch, but the vias are still of manufacturing reasons provided with a small circular metal disk at their tops. The geometry of the final unit cell and the corresponding dispersion diagram defining the stopband is shown in Fig. 4. The dispersion diagram is calculated using CST Eigen mode solver for a unit cell surrounded by periodic

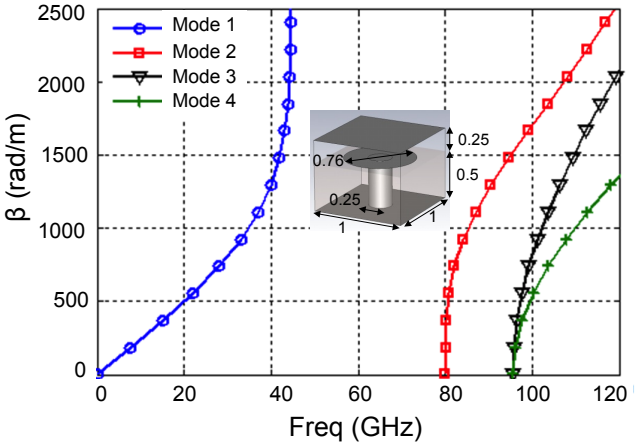

Fig. 4. Dispersion diagram of the periodic surface of metalized via holes with a circular disk on top used to create the stopband of the parallel-plate modes.

boundaries. It is observed that the metallized vias provide a stopband over 44.5 to 80 GHz covering the operational bandwidth with good margins. The stopband of the parallel-plate modes is larger when the height of the air gap (h_g) is

TABLE I. THE MATERIALS USED AS SUBSTRATE IN THE DESIGNED 2×2-slot SUBARRAY

Upper PCB	
Material	Rogers RT/Duroid 5880
Dielectric constant	2.2
Loss tangent	0.0009
Thickness (mm)	0.78
Lower PCB	
Material	Rogers RO3003
Dielectric constant	3
Loss tangent	0.0013
Thickness (mm)	0.5

smaller. At the same time this height determines the characteristic impedance of the microstrip-ridge gap waveguide together with the line width. In addition, the conductive losses are smaller when the line width and air gap are larger. Therefore, we chose the line width to be as large as possible but without being so large that higher order strip-modes are excited, and at the same time keeping the stopband large enough with margins with respect to the band of operation.

The upper textured surface of the lower PCB can be designed based on the principles of gap waveguides discussed in [6-10]. Rogers Ro3003 with loss tangent of 0.0013, thickness of 0.5mm and characteristics given in Table I was chosen as the substrate. The thickness is close to $\lambda_0/4\sqrt{\varepsilon_r}$. Then the parameters "$p$", "$p_a$", and "$d_p$" in Fig. 3(b) were tuned so that the parallel-plate stopband covers the operating frequency with margins.

The design of the microstrip-ridge gap waveguide distribution network itself is not part of this paper. It can have different shapes depending on bandwidth requirements.

A short piece of the microstrip-ridge gap feed line, as illustrated in Fig. 3 (b), was included in the optimizations of the 2×2-slot subarray. The dimensions used to tune the S_{11} and radiation characteristics are shown in Fig. 3(b). The final values of these dimensions can be found in Table II in Sec. III.

C. *Optimizing the radiating unit cell dimension*

In order to obtain highest aperture efficiency and widest bandwidth the 2×2-slot element dimensions were optimized. It is well known that the slots (or other elements) in an antenna aperture should be uniformly spaced in both x and y directions with spacing smaller than one wavelength in order to avoid grating lobes in large broadside arrays. For finite-sized arrays of diameter D (in our case D=Nl where N is the number of subarrays), this element spacing d_s (in our case d_s is equal to w/2 and l/2 in E- and H-planes respectively) should even be smaller than one wavelength in order to avoid grating lobes along the ground plane, satisfying

$$\frac{d_s}{\lambda} < \frac{1}{1+(\lambda/D)} \tag{1}$$

as explained in [24, Eqs. (10.26) and (10.79)]. This latter stricter requirement may be relaxed if the element pattern has a null along the ground plane, such as in H-plane of slots. In E-plane we must strictly adhere to it because slots have

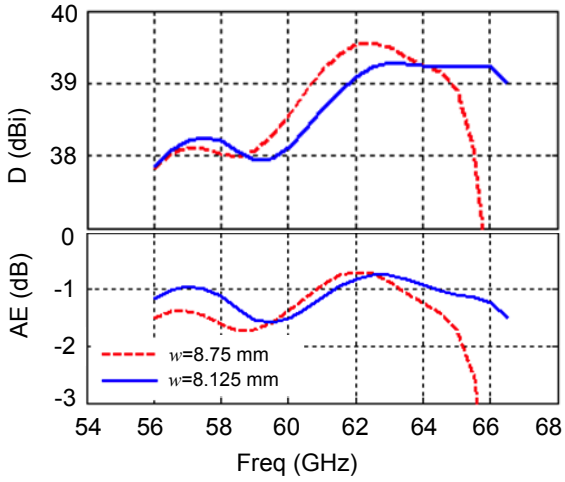

Fig. 5. Effect of unit cell dimensions and consequently slot spacing on aperture efficiency and directivity for the case without SIW corrugations. The results were computed for a 32×32 slot array.

uniform radiation pattern in E-plane. At the same time we do not want to make the element spacing smaller than necessary, in order to keep the total aperture size of the array as large as

possible, to obtain the highest possible directivity from a given number of elements.

In order to satisfy the above conditions we optimized the unit cell dimensions "l" and "w" as well as the inter-element slot spacing within the 2×2-slot subarray. It should be noted that the slot dimensions "w_s" and "l_s" as well as the coupling slot sizes "w_c" and "l_c" were tuned at the same time to achieve good impedance matching over the operating bandwidth. Fig. 5 shows the effect of unit cell dimensions and consequently the slot spacing, on aperture efficiency and directivity of a 32×32 slot array. In this figure, the aperture efficiency (AE) is defined as "D/D_{max}" where "D" is the antenna directivity obtained from HFSS (with infinite array approach) and "D_{max}" is the maximum available directivity from the aperture obtained by using $4\pi A/\lambda^2$ where $A=(16\times16)wl$ is the area of antenna aperture. It is observed that for the larger unit cell and consequently larger spacing between the slots, the aperture efficiency is lower in most of the band, but the directivity is higher due to the larger physical aperture area of the total array, except at the higher part of the frequency band there grating lobes starts to appear along the ground plane so that the directivity as well as aperture efficiency drops severely. The results in Fig. 5 were obtained without the SIW corrugations.

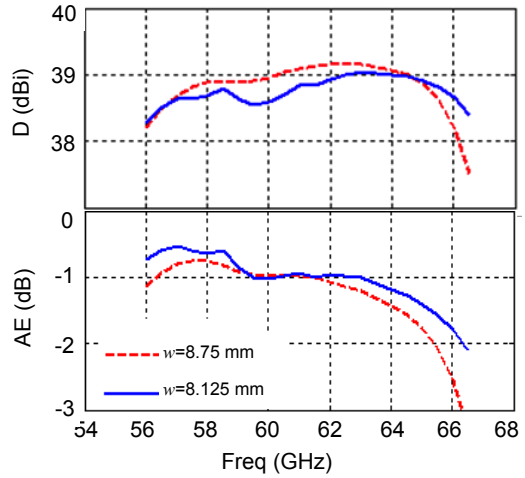

Fig. 6. Effect of unit cell dimensions and consequently slot spacing on directivity (D) and aperture efficiency (AE) for the case with SIW corrugations. The results were computed for a 32×32 slot array.

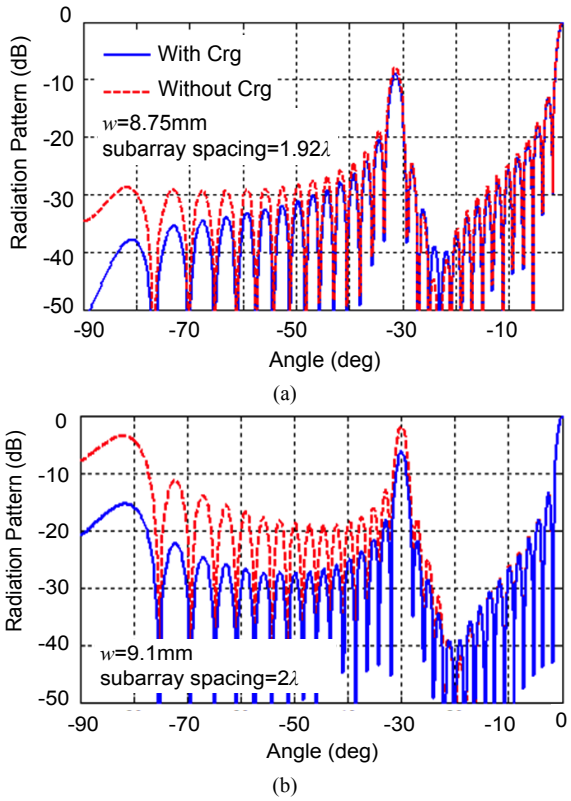

Fig. 7. The SIW corrugations potential for directivity enhancement. The E-plane radiation pattern is plotted @ 66 GHz for the two cases of with and without corrugations. (a). Unitcell width "w" is 8.78mm i.e. subarray spacing is less than but very close to two wavelengths (b). Unitcell width "w" is 9.1mm i.e. subarray spacing is exactly two wavelengths.

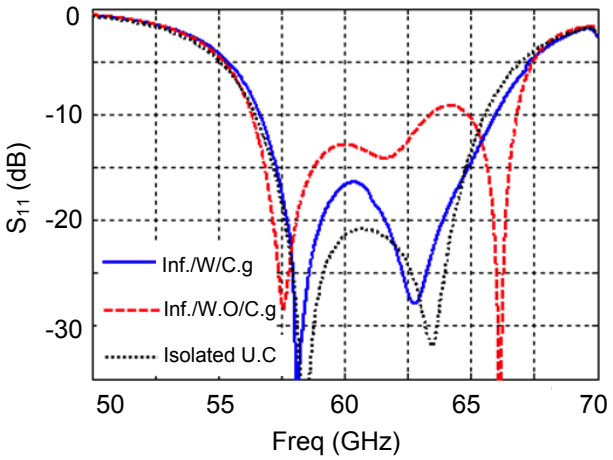

Fig. 8. Effect of SIW corrugation on reflection coefficient. The solid line is S_{11} for the case of infinite array with corrugations, the dashed line is S_{11} for the case of infinite array without corrugations, and the dotted line is S_{11} for the case of an isolated unit cell without corrugations and on an infinite ground plane.

D. The SIW-corrugations

The SIW technology in the upper PCB made it easy to implement SIW corrugations between each 2×2-slot subarray in E-plane., working as a soft surface with similar effect as an EBG surface, as discussed in the Introduction. Thereby, we could suppress the mutual coupling between subarrays and this made it easier to impedance match the S_{11} in the infinite array environment. At the same time there will be a null in the subarray pattern along the ground plane, and thereby the grating lobe problem was reduced. The SIW corrugations in the upper PCB are illustrated in Fig. 1. It is observed that each SIW corrugation appears as a dielectric-filled longitudinal cavity under a long slot and with via hole walls, filling the space between neighboring subarrays.

The substrate of the upper PCB is Rogers 5880 with thickness of 0.78mm and characteristics given in Table I. The thickness is close to $\lambda_0/4\sqrt{\varepsilon_r}$, making it easy to design the SIW corrugations for operation as a wideband soft surface in E-plane .The corrugation width "d_c" was tuned in order to improve the performance of the antenna in terms of bandwidth of S_{11} and directivity.

In Fig. 6 the same investigation as in Fig. 5 is done for the

case with SIW corrugations. By comparing the directivity curves in Fig. 5 and Fig. 6 we see that the drop in directivity at high frequency for the larger element spacing, is much smaller with SIW corrugation than without. Thus the grating lobe problem pointed out in paragraph C has been reduced. We still had to choose the smaller element spacing to avoid the directivity drop almost completely at 66 GHz. As a result, the directivity is almost constant with frequency when using SIW corrugations, whereas it without the SIW corrugation is significantly lower below 60 GHz than above.

TABLE II. DIMENSIONS OF DESIGNED 4 SLOT SUBARRAY (UNITS: mm)

Para.	value	Para.	value
l	8.75	d_p	0.559
w	8.125	d_c	1.063
w_s	1.414	w_f	1.11
l_s	2.494	p_a	0.762
d	2.1	p	0.254
w_c	1.2	d_p'	1
l_c	2.45	d_f	1
a_1	1.112	c	0.451
a_2	0.8128	t	0.387
p	0.254	t'	0.25
		h_g	0.25

In Fig. 7 the E-plane radiation pattern of a 32×32 slot array at 66 GHz is illustrated, for the two cases with and without SIW corrugations and for two element spacings. We see a high grating lobe at 31° from broadside, which is caused by asymmetric excitation of the 2×2-slots within each subarray. The SIW corrugations affect the far-out sidelobes being associated with the second grating lobe starting to appear along the ground plane at 90° from broadside. We see clearly how the sidelobes are reduced by using the SIW corrugations, and additionally by reducing the element spacing "w". In Fig. 7(a), the directivity for the two cases with and without corrugations was 38.2 dBi and 36.2 dBi, respectively, in agreement with Fig. 5(a) and Fig. 6(a). At least part of this improvement is due to the far-out sidelobes, because there was also an improvement in the level of the first gating lobe when using SIW corrugations. As a result, using SIW corrugations gives the potential to use larger slot spacing closer to one wavelength and consequently achieving higher directivity.

The 2×2-slot subarrays are not surrounded by corrugations in H-plane (xz plane) since the mutual coupling in this direction is negligible and the element pattern already has a null at 90°.

We also investigated the effect of SIW corrugations on the reflection coefficient S_{11}, see Fig. 8, where S_{11} is shown for the three cases: infinite array with corrugations, infinite array without corrugations, and isolated unit cell without SIW corrugations and with an infinite ground plane outside. Note that for each case the geometry was tuned for the best possible impedance matching. The curves show that S_{11} for the case of infinite array with corrugations is very similar to that of the isolated unit cell. This fact reveals that the SIW corrugations have suppressed mutual coupling between 2×2-slot subarrays and this made it much easier to match the reflection coefficient to acceptable performance within the desired frequency band.

TABLE III. COMPARISON OF MISMATCH FACTOR (MF), IMPEDANCE BANDWIDTH (BW), DIRECTIVITY (D) AND SUBARRAY OHMIC LOSS FOR TWO CASES OF WITH AND WITHOUT CORRUGATIONS

Without corrugations			
BW(-10 dB) BW(-15 dB)		12.4% 3.41%	
Freq (GHz)	MF (dB)	D (dBi)	Subarray ohmic loss (dB)
57	-0.0853	38.21	4.43×10^{-5}
58	-0.0329	38.19	4.27×10^{-5}
61.5	-0.1702	38.87	1.32×10^{-5}
63	-0.3685	39.28	2.77×10^{-5}
65	-0.4125	39.22	2.11×10^{-6}
66	-0.0133	39.21	7.28×10^{-6}
With corrugations			
BW(-10 dB) BW(-15 dB)		16.8% 13.6%	
Freq (GHz)	MF (dB)	D (dBi)	Subarray ohmic loss (dB)
57	-0.2543	38.62	6.57×10^{-6}
58	-0.0066	38.68	2.89×10^{-6}
61.5	-0.0480	38.82	2.09×10^{-5}
63	-0.0087	39	3.21×10^{-5}
65	-0.1598	38.9	4.61×10^{-5}
66	-0.4813	38.64	2.48×10^{-5}

III. Simulated Results of 32×32 Array Using Infinite Array Approach

The designed 2×2-slot subarray with the dimensions listed in Table II was simulated by using the infinite array approach, and by including the conductivity of Copper and the actual permittivity and loss tangents of the substrate materials. The reflection coefficient S_{11} and radiation patterns are presented for a sample 32×32 array i.e. 16×16 array of 2×2-slot subarrays.

A. Subarray reflection coefficient

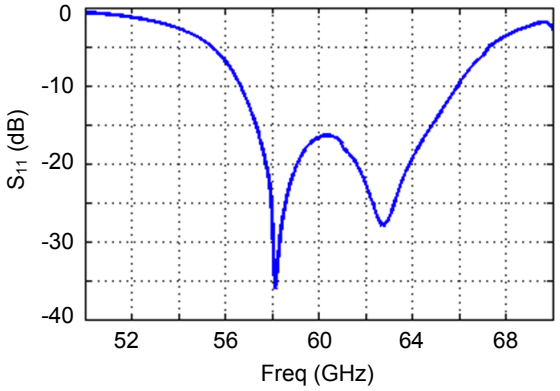

Fig. 9. Reflection coefficient of designed 2×2-slot subarray with periodic walls.

Fig. 9 shows the reflection coefficient S_{11} seen at the microstrip-ridge gap waveguide port of the subarray. We see that the bandwidth for S_{11} < -10dB is 16.8% (56.5~66 GHz), and it is 13.6% (57.2~65 GHz) for $S_{11}\leq$ -15dB. For comparison, the 2×2-slot subarray presented in [5] has correspondingly 11.8% (58.1~65 GHz) and 8.8% (59~64.2 GHz) bandwidths.

In Table III the mismatch factor MF (defined as 1-$|S_{11}|^2$) and the S_{11} bandwidth are compared for the two cases with and without corrugations. The directivities and the ohmic loss in the subarray are also shown. The latter is negligible.

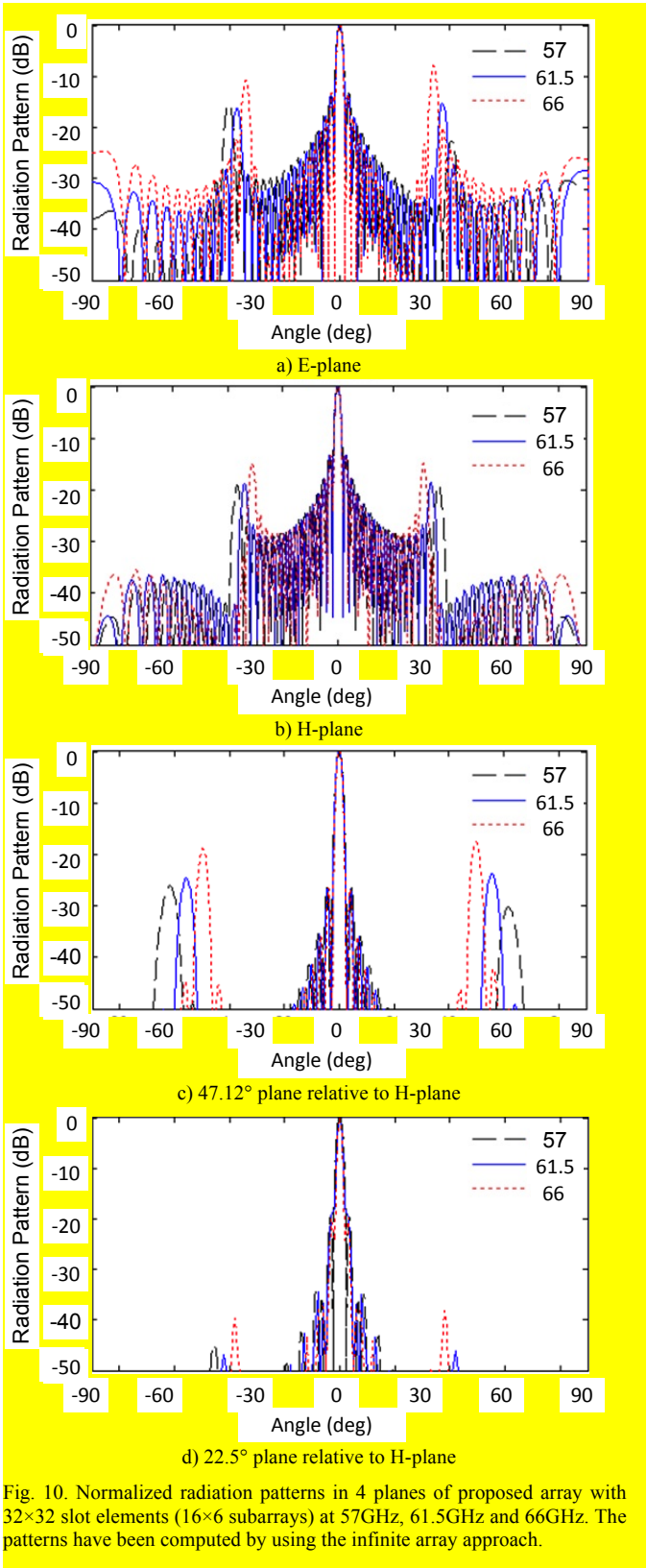

Fig. 10. Normalized radiation patterns in 4 planes of proposed array with 32×32 slot elements (16×6 subarrays) at 57GHz, 61.5GHz and 66GHz. The patterns have been computed by using the infinite array approach.

B. *Radiation pattern*

The radiation patterns were computed with CST microwave Studio using also periodic boundary conditions around the same subarray. (The reason was that we detected a problem with HFSS so we have contacted them to sort that out.)

In Fig. 10 the radiation patterns of the 32×32 slot array aperture are given in 4 planes for the end and center frequencies of the band. In Fig. 10 (a) we observe grating lobes appearing at around 30° due to the periodic spacing between the subarrays, both in E- and H-planes. This is caused by an asymmetry due to higher order modes present in the radiating slots, and they will create a variation along the whole array with the same period as that of the subarrays. The reason is that the feed line and coupling slot are not able to couple equally to all 4 radiating slots of the subarray, in spite of the fact that the geometry of the cavity has two planes of symmetry. In fact, as shown in Fig. 3(a), the microstrip-ridge line and the coupling slot has an inherently asymmetry in E-plane direction, and this may cause higher order E-plane modes in the coupling slot that excite the two upper slots in Fig. 3(a) differently from the two lower ones. The grating lobes in H-plane are also much lower because this asymmetry of the excitation of the coupling slot is not present in H-plane.

The appearances of the grating lobes are determined by the subarray spacings in E-plane and H-plane, according to [24]. This gives

$$\theta = \sin^{-1}(\lambda / w) \text{ and } \theta = \sin^{-1}(\lambda / l) \qquad (2)$$

in E- and H-planes, respectively, where w and l are given in Table II and Fig. 3(a), and λ is the wavelength. According to the same classic array theory there will also be grating lobes appearing in a an azimuth plane and polar angle determined by

$$\phi = \arctan(l / w) \ \& \ \theta = \sin^{-1}\left(\sqrt{(\lambda / w)^2 + (\lambda / l)^2}\right) \qquad (3)$$

respectively. The ϕ-plane becomes 47.12° by using the values of w and l in Table II. This corresponds to the complementary diagonal plane of the geometry, because the diagonal plane in Fig. 3 is given by arctan(w/l). The radiation patterns in the 47.12° plane are shown in Fig. 10 (c), showing very high grating lobes. We have verified that these lobes are very narrow and have a maximum in the 47.12° plane, so the classical theory works. However, the lobes are much higher than expected, and this may be an undesired effect of the SIW corrugations and need to be investigated later. We have also shown the sidelobes in the 22.5° plane in Fig. 10 (d) and these are seen to be very low.

The simulated radiation characteristics of the 32×32 slot array aperture are summarized in Table IV. We have also tabulated the locations of the grating lobes in the different planes, and we see that the locations read from the curves agree with those obtained from equations (2)-(3) above. The indexes ”SLL”, ”HPBW” and “GL” are abbreviations for ”side lobe level”, ”half power beam width” and “grating lobes” respectively. The grating lobes efficiency is representing the reduction in directivity due to the power lost in the grating lobes and is calculated based on the formula presented in [24, Eq. (10.91)]. For broadside radiation, this formula is reduced to

$$GL_{efficiency} = \left\{ 1 + \sum_{all\ g} \frac{|GL(\theta_g,\phi_g)|}{\cos\theta_g} \right\}^{-1} \quad (4)$$

In above formula $|GL(\theta_g,\phi_g)|$ is the absolute value of the grating lobe (GL) located at (θ_g,ϕ_g) relative to the maximum of the main beam, extracted from the normalized power radiation pattern of the antenna. In Table IV, the GL efficiency is calculated for the first grating lobes in E-, H-, +47.12° plane and -47.12° plane, i.e. the GL efficiency shows the losses due to the first grating lobes on both sides of the main lobe in E-, H-, +47.12° and -47.12° planes. The lobes in the -47.12° plane are the same as in the +47.12° plane of symmetry reasons. Thus, the GL efficiency formula has in total 8 contributing grating lobes. The table shows also the aperture efficiency of the array computed from the maximum available directivity of such an aperture size, and the computed directivity from the infinite array approach. We see that GL efficiency formula in (4) predicts GL efficiencies that are very close to and a bit higher than the aperture efficiencies, which is reasonable.

We computed also the directivities of 16×16-slot arrays and 8×8-slot arrays using the same subarray and the infinite array approach. The aperture efficiencies computed from the simulated directivities were the same, so the designed subarray can also be used for directive arrays of different sizes.

TABLE IV. RADIATION CHARACTERISTICS OF PROPOSED ARRAY WITH 32×32-SLOT ELEMENTS

Freq (GHz)	57	61.5	66
Maximum available directivity from aperture of this size (dBi)	39.16	39.82	40.44
Directivity from simulation (dBi)	38.64	39.06	38.52
Aperture efficiency (dB)	-0.52	-0.76	-1.92
HPBW E-plane (deg)	2.00	1.89	1.74
HPBW H-plane (deg)	1.9	1.76	1.64
1st SLL E-plane (dB)	-13.23	-13.3	-13.37
1st SLL H-plane (dB)	-13.31	-13.4	-13.34
Location E-plane GL			
➢ From formula	40.37	36.9	34
➢ From simulation	40.5	37.25	34.2
Level E-plane GL (dB)	-15.6,-22.7	-16.2,-15.2	-8,-10.8
Location H-plane GL			
➢ From formula	36.97	33.85	31.29
➢ From simulation	36.5	33.75	31
Level H-plane GL (dB)	-19	-18.7	-14.9
Location 47.12°-plane GL			
➢ From formula	62.12	55.01	49.76
➢ From simulation	61.75	55.75	49.75
Level 47.12°-plane GL (dB)	-26,-30.2	-24.5,-23.7	-17.6,-19
GL efficiency (dB)	-0.37	-0.52	-1.64

IV. VALIDATION USING SMALL 4×4 SLOT ARRAY

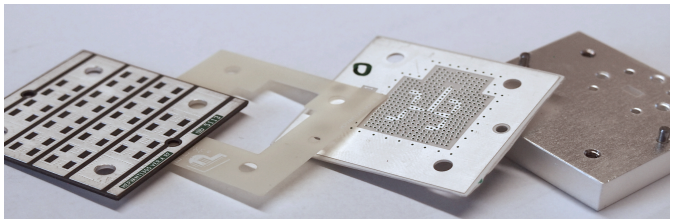

Fig. 11. Photo of the disassembled fabricated 4×4 slot array (surrounded by some dummy slots). From left to right: The upper radiating PCB, a dielectric spacer defining the air gap, the microstrip-ridge gap waveguide distribution network, and a thick metal support plate with a WR15 flange in it.

We decided to build a small array consisting of 4×4 slots, i.e. a 2×2 array of 2×2-slot subarrays. This array is too small to verify the design approach regarding the element spacing and grating lobe suppressions. However, it is large enough to validate if we have good control of the radiation characteristics using HFSS, and the effect of the SIW corrugations. The distribution network is fully branched feeding all 2×2 subarrays with equal amplitude and phase. It is realized in microstrip-ridge gap waveguide with a 90° transition to WR15 rectangular waveguide fixed to the back side of the lower PCB. The WR15 transition is described in [25], and the corporate feed network will be described in a later article about the full 32×32 array.

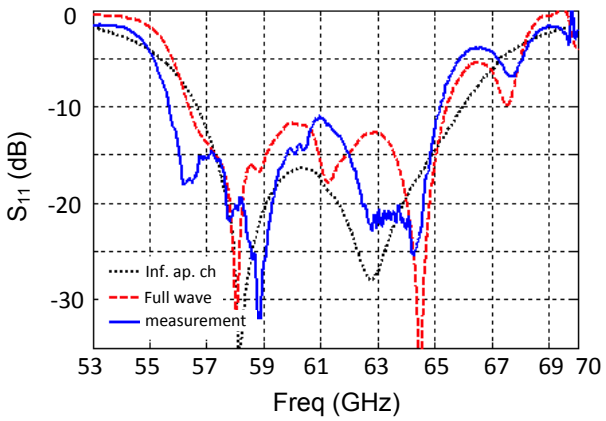

Fig. 12. Reflection coefficient of 4×4 slot array antenna. Solid line and dashed line are s_{11} of 4×4 slot array obtained by measurement and full wave simulation respectively. Dotted line is s_{11} for a 2×2 slot subarray in infinite array.

The final dimensions of the unit cell are listed in Table II. The materials used as the substrates in the upper and lower PCBs and their properties are listed in Table I.

The constructed antenna is illustrated in Fig. 11. The centered 4×4 slot array is excited by the corporate feed network and the other surrounding slots are dummy elements. In Fig. 12 the reflection coefficient of the full 4×4 slot array (including surrounding dummy elements) is compared with that of the 2×2-slot subarray in an infinite array environment. We see good agreement between full wave simulation, infinite approach and measured results. The full wave simulation shows that the impedance is matched (S_{11}≤-10dB) for the frequency range of 56.37-65.43 GHz (16%), which is very

close to the result obtained by the infinite array approach. The measured result shows that the impedance is matched for 55.68-65.17 GHz (17%), which is in good agreement with the full wave simulations based on the infinite array approach.

The simulated and measured E- and H-plane radiation patterns of the validation antenna are illustrated at three frequencies. We observe quite good agreement between the simulated and measured radiation patterns. Table V summarizes the most important features shown in Figs. 12 and 13. The table shows also the directivities and the aperture efficiencies compared to an aperture size of $4wl$, i.e. the aperture without the dummy subarrays. We see that even though this test array is very small, the simulated directivities with the infinite array approach and the full wave approach are quite close, except at 66 GHz. Thus, the infinite array approach is useful even when designing small arrays of 4×4 elements, and in particular when the radiating part of the arrays is surrounded by dummy elements in order to reduce the effect of the finiteness of the array. We also see by comparing with Table IV that the aperture efficiencies for the infinite array approach are the same as the ones we have for the 32×32 slot array.

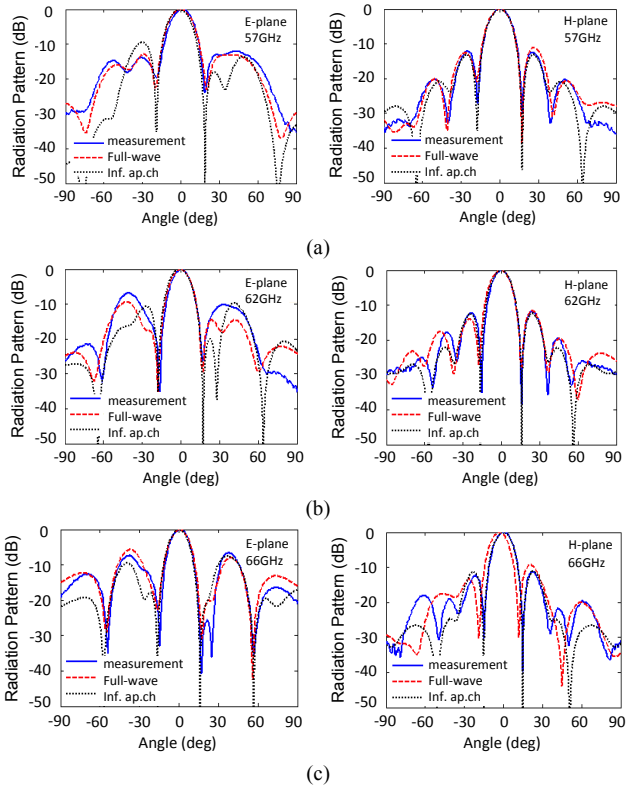

Fig. 13. Radiation patterns of 4×4 slot array antenna in E- and H-planes @ (a). 57GHz (b). 62GHz and (c). 66GHz. In each plot the results of full wave simulation and measurement of 4×4 slot array is compared with that obtained by infinite array approach on 2×2 slot subarray.

We should mention here that the PCBs that were manufactured first had a standard coating of ENIG, i.e. Electroless Nickel / Immersion Gold, on all Copper traces and pads. This ENIG layer caused a large attenuation and a frequency shift of S_{11}, see [25] for more explanations about the problems with the ENIG layer. Thus, the ENIG coating cannot be used on PCBs used for gap waveguides. The reason is that the currents on the microstrip-ridge gap lines float on the air-interface of the Copper trace, and not on the interface to the substrate like in normal microstrip lines. The final measured prototypes has a thin Silver coating on all Copper traces, seen by the Silver color on the photo in Fig. 11. The measured radiation patterns of the first model were in agreement with the simulations even with the ENIG layer.

V. CONCLUSION

We have developed a subarray to be used in a planar slot array antenna with high efficiency at 60 GHz. It is realized using two double-sided PCBs separate by an air gap containing the quasi-TEM microstrip-ridge gap waveguide modes of the distribution network. The upper PCB contains radiating slots backed by SIW cavity. Using gap waveguide and SIW technologies together, has made the proposed antenna attractive from the manufacturing point of view especially at millimeter wave band. In addition, application of SIW corrugations between the subarrays in the upper PCB has resulted in the suppression of mutual coupling and consequently a wider bandwidth of the reflection coefficient.

The 32×32 array show grating lobes in E-, H- and the complementary diagonal plane (47.12°) of the geometry. These appear where they should be according to classic array antenna theory, and also their levels are in agreement with that. According to classical theory the sidelobes in the diagonal planes should in dB be a sum of the corresponding grating lobes in the two principle planes.

A sample 4×4 slot array antenna for operation at 60 GHz was fabricated to verify the design approach. This was realized by using a 2×2 distribution network in microstrip-ridge gap waveguide, and we used dummy subarrays around it to reduce the edge effects. The radiation patterns for this small array show high sidelobes in E- and H-planes, because the grating lobes and the first sidelobes coincide. The input S_{11} of the 4×4 array is below -10 dB over a 17% bandwidth. However, the most important is that we have good agreement between simulations and measurements, and therefore we know that the design is valid and will work in a larger array with the simulated large-array performance, provided the distribution network can be realized. This will be the focus of a later article.

TABLE V. SUMMARY OF IMPORTANT FEATURES OF 4×4 SLOT ARRAY SHOWN IN FIGS. 12 AND 13. "NA means not available"

Infinite array approach				
BW(-10 dB)	16.8% (56.5-66 GHz)			
Freq (GHz)	E plane SLL (dB)	H plane SLL (dB)	Directivity (dBi)	Aperture efficiency (dB)
57	-9.6	-13	20.58	-0.52
62	-9.76	-12.48	21	-0.76
66	-7.6	-11.3	20.45	-1.92
Full-wave approach				
BW(-10 dB)	16% (56.37-65.43 GHz)			
Freq (GHz)	E plane SLL (dB)	H plane SLL (dB)	Directivity (dBi)	Aperture efficiency (dB)
57	-13.17	-11.1	20.68	-0.42
62	-9.4	-11.55	21.13	-0.63
66	-5.7	-9.3	19.94	-2.43
Measurement				
BW(-10 dB)	12.1% (61.9-69.43 GHz)			
Freq (GHz)	E plane SLL (dB)	H plane SLL (dB)	Directivity (dBi)	Aperture efficiency (dB)
57	-12	-12.2	NA	NA
62	-6.83	-11.87	NA	NA
66	-6.6	-11.31	NA	NA

REFERENCES

[1] S. S. Oh, J. W. Lee, M. S. Song, and Y. S. Kim, "Two-layer slotted waveguide antenna array with broad reflection/gain bandwidth at millimetre-wave frequencies," *IEE Proc.-Microw. Antennas Propag.*, vol. 51, no. 5, pp. 393–398, Oct. 2004.

[2] Y. Kimura, Y. Miura, T. Shirosaki, T. Taniguchi, Y. Kazama, J. Hirokawa, and M. Ando, "A low-cost and very compact wireless terminal integrated on the back of a waveguide planar array for 26 GHz band fixed wireless access (FWA) systems," *IEEE Trans. Antennas Propag.*, vol. 53, no. 8, pp. 2456–2463, Aug. 2005.

[3] S. Park, Y. Tsunemitsu, J. Hirokawa, and M. Ando, "Center feed single layer slotted waveguide array," *IEEE Trans. Antennas Propag.*, vol. 54, no. 5, pp. 1474–1480, May 2006.

[4] K. Jung, H. Lee, G. Kang, S. Han, and B. Lee, "Cavity-backed planar slot array antenna with a single waveguide-fed subarray," in *Proc. IEEE Antennas Propag. Soc. Int. Symp., 115.5*, Jun. 2004.

[5] Y. Miura, J. Hirokawa, M. Ando, Y. Shibuya and G. Yoshida, "Double-layer full -corporate-feed hollow-waveguide slot array antenna in the 60 GHz band," *IEEE Trans. Antennas Propag.*, vol. 59, no. 8, pp. 2844–2851, Aug 2011.

[6] P. S. Kildal, E. Alfonso, A. Valero-Nogueira, and E. Rajo-Iglesias, "Local metamaterial-based waveguides in gaps between parallel metal plates," IEEE Antennas and Wireless Propagation Letters, vol. 8, pp. 84–87, 2009.

[7] P. S. Kildal, "Waveguides and transmission lines in gaps between parallel conducting surfaces," European patent application No. PCT/EP2009/057743, 2009.

[8] P. S. Kildal, "Three metamaterial-based gap waveguides between parallel metal plates for mm/submm waves," in 3rd European Conference on Antennas and Propagation (EuCAP 2009), pp. 28–32.

[9] P. S. Kildal, A. U. Zaman, E. Rajo-Iglesias, E. Alfonso, and A. Valero-Nogueira, "Design and experimental verification of ridge gap waveguide in bed of nails for parallel-plate mode suppression," IET Microwaves, Antennas and Propagation, vol. 5, no. 3, pp. 262–270, 2011.

[10] A. U. Zaman, A. Kishk, and P.-S. Kildal, "Narrow-band microwave filter using high Q groove gap waveguide resonators without sidewalls", IEEE Transactions on Components, Packaging and Manufacturing Technology, Vol. 2, No. 11, pp. 1882-1889, November 2012.

[11] A. Valero-Nogueira, M. Baquero, J. I. Herranz, J. Domenech, E. Alfonso, and A. Vila, "Gap waveguides using a suspended strip on a bed of nails," IEEE Antennas and Wireless Propagation Letters, vol. 10, pp. 1006–1009, 2011.

[12] E. Pucci, E. Rajo-Iglesias, P.-S. Kildal, "New Microstrip Gap Waveguide on Mushroom-Type EBG for Packaging of Microwave Components", IEEE Microwave and Wireless Components Letters, Vol. 22, No. 3, pp. 129-131, March 2012.

[13] E. Rajo-Iglesias, P.-S. Kildal, "Numerical studies of bandwidth of parallel plate cut-off realized by bed of nails, corrugations and mushroom-type EBG for use in gap waveguides", IET Microwaves, Antennas & Propagation, Vol. 5, No 3, pp. 282-289, March 2011.

[14] H. Raza, J. Yang, P.-S. Kildal, E. Alfonso, "Resemblance Between Gap Waveguides and Hollow Waveguides", IET Microwaves, Antennas & Propagation, Volume 7, Issue 15, 10 December 2013, p. 1221 – 1227.

[15] P.-S. Kildal, A. A. Kishk, and S. Maci, "Special issue on artificial magnetic conductors, soft/hard surfaces, and other complex surfaces" (Guest Editorial), IEEE Transactions on Antennas and Propagation, vol. 53, no. 1, pp. 2-7, Jan. 2005.

[16] R. Li, G. DeJean, M. M. Tentzeris, J. Papapolymerou, J. Laskar, "Radiation-pattern improvement of patch antennas on a large-size substrate using a compact soft-surface structure and its realization on LTCC multilayer technology", IEEE Trans. Antennas Propagat., Vol. 53, No. 1, pp. 200-208, Jan. 2005.

[17] E. Rajo-Iglesias, O. Quevedo-Teruel L. Inclan-Sanchez, "Mutual coupling reduction in patch antenna arrays by using a planar EBG structure and a multilayer dielectric substrate", IEEE Trans. Antennas Propagat., Vol. 56, No. 6, pp. 1648-1655, June 2008.

[18] E. Pucci, E. Rajo-Iglesias, J.-L. Vazquez-Roy and P.-S. Kildal, "Planar Dual-Mode Horn Array with Corporate-Feed Network in Inverted Microstrip Gap Waveguide", submitted to IEEE Transactions on Antennas and Propagation, Aug. 2013.

[19] A. U. Zaman and P. S. Kildal, "Wideband slot antenna array with single-layer corporate feed-network in ridge gap waveguide technology", submitted to IEEE Transactions on Antennas and Propagation, June 2013.

[20] G. Q. Luo, Z. F. Hu,Y.Liang,L.Y.Yu, and L. L. Sun, "Development of low profile cavity backed crossed slot antenna for planar integration," *IEEE Trans. Antennas Propag.*, vol. 57, no. 10, pp. 2972–2979, Oct. 2009.

[21] F. Xu and K. Wu, "Guided-wave and leakage characteristics of substrate integrated waveguide," *IEEE Trans. Microw. Theory Tech.*, vol. 53, no. 1, pp. 66–73, Jan. 2005.

[22] G. Q. Luo, W. Hong, Q. H. Lai, K. Wu, and L. L. Sun, "Design and experimental verification of compact frequency selective surface with quasi-elliptic bandpass response," *IEEE Trans. Microw. Theory Tech.*, vol. 55, no. 12, pp. 2481–2487, Dec. 2007.

[23] H. Uchimura, T. Takenoshita, and M. Fujii, "Development of a 'laminated waveguide'," *IEEE Trans Microw. Theory Tech.*, vol. 46, no. 12, pp. 2438–2443, Dec. 1998.

[24] P. -S. Kildal, *Foundations of Antennas: a Unified Approach for Line-of-Sight and Multipath*, Compendium (draft textbook) available from the author, Spring 2013.

[25] H. Raza, J. Yang, P-S. Kildal and E. Alfonso, "Microstrip-Ridge Gap Waveguide – Study of Losses, Bends and Transition to WR-15", submitted to Transactions on Microwave Theory and Techniques, 9th December, 2013.